Polymer-Controlled Morphosynthesis and Mineralization of Metal Carbonate Superstructures†

Shu-Hong Yu,‡ Helmut Cölfen,§ and Markus Antonietti*

Max Planck Institute of Colloids and Interfaces, Department of Colloid Chemistry, MPI Research Campus Golm, D-14424 Potsdam, Germany, and Department of Materials Science and Engineering and Structure Research Laboratory of CAS, University of Science and Technology of China, Hefei 230026, P. R. China

Received: January 2, 2003; In Final Form: April 11, 2003

Different morphosynthesis strategies for various metal carbonate minerals such as $CaCO_3$, $BaCO_3$, $CdCO_3$, $MnCO_3$, and $PbCO_3$ using double hydrophilic block copolymers (DHBCs) as crystal modifiers are presented. The influence of the DHBCs with different functionalities such as carboxyl, partially phosphonated, and phosphorylated groups on the crystallization and structure formation was investigated. Well-defined crystals with size range from mesoscale to microscale can be easily obtained. More complex higher-order superstructures such as hollow spheres and big spherules with controlled surface structures can also be assembled conveniently. The results show that polymer-controlled mineralization is a versatile tool toward crystal morphogenesis. A time-dependent self-assembly and growth of "sphere-to-rod-to-dumbbell-to-sphere" structures was observed in the case of $BaCO_3$ under the control of DHBCs, adding to the already reported examples of $CaCO_3$ and fluoroapatite. In addition, we found that the influence of the DHBCs while increasing the ionic strength was lost in case of $CaCO_3$, implying that the strong selective interaction between the functional groups of DHBCs and crystals has electrostatic contributions.

1. Introduction

Bioinspired morphosynthesis strategies, using self-assembled organic superstructures to template inorganic materials with controlled morphologies, have received a lot of attention.[1] For this biomimetic synthesis of inorganic materials with complex form, organic additives and/or templates with complex functionalization patterns are used to control the nucleation, growth, and alignment of inorganic crystals.[1]

Calcium carbonate ($CaCO_3$) is one of the standard model systems due its abundance in nature and also its important industrial application in paints, plastics, rubber, or paper.[2] $CaCO_3$ has three anhydrous crystalline polymorphs which have typical morphologies: calcite (rhomboeder), aragonite (needles), and vaterite (polycrystalline spheres). In addition, amorphous $CaCO_3$ (ACC) is known, as well as crystalline mono- and hexahydrates. Calcite and aragonite are by far the most common polymorphs, whereas vaterite, a less stable polymorph, is not commonly formed by organisms.[3,4]

Biomimetic synthesis of $CaCO_3$ crystals in the presence of organic templates and/or additives has been intensively investigated in recent years as reviewed recently.[5] Langmuir monolayers,[6−10] ultrathin organic films,[11] self-assembled films,[12−14] and foam lamellae[15] have been used as effective templates for the controlled growth of $CaCO_3$ crystals, focusing on the control of the polymorph and crystal orientation. Cross-linked gelatine films,[16,17] polymer substrates,[2] crystal-imprinted polymer surfaces,[18] and polymeric matrixes[19,20] have also been employed to direct the controlled growth of $CaCO_3$ crystals. It has been shown that special functional low molecular weight and polymeric additives can influence the crystallization of $CaCO_3$ strongly,[21−23] including complex liquidlike morphologies[24,25] or stabilized amorphous $CaCO_3$.[26,27]

$CaCO_3$ films have been successfully prepared in the presence of both organic substrates and soluble polymeric additives.[28,29] The protein macromolecules isolated from mollusk shells[3,30,31] and intracrystalline macromolecules from sea urchin spines[32] or ascidian skeletons[33] have shown distinct control on the polymorph of $CaCO_3$ crystals. Interestingly, a designed peptide has been synthesized and used for the conformation-dependent control of the calcite morphology.[4] In addition, a combinatorial approach was successfully applied to select the most active peptides for $CaCO_3$ crystallization out of a library.[34] In a recent report, Au nanocolloids were successfully used as nuclei for the crystallization of $CaCO_3$,[35] and Tremel et al showed by that approach that micrometer-sized (10 μm) spherules with well-defined surface structures displaying complex aggregates of faceted calcite crystals can be obtained.[36]

Recently, a new class of functional polymers, the so-called double-hydrophilic block copolymers (DHBCs),[37−39] was developed for mineralization purposes. These polymers consist of one hydrophilic block designed to interact strongly with the appropriate inorganic minerals and surfaces and another hydrophilic block that does not interact (or only weakly and mainly promotes solubilization in water). The potential of polyacrylate in nucleation and growth processes was identified rather early by the pioneering work of Henglein and co-workers.[40−42] Owing to the separation of the binding and the solvating moieties, DHBCs are "improved versions" of the polyacrylate and turned out to be extraordinarily effective in crystallization control for calcium carbonate.[43−47] For example, calcite or vaterite spheres, twins, and hollow spheres were obtained.[43,45] Complex mor-

* To whom correspondence should be addressed. E-mail: antonietti@mpikg-golm.mpg.de. Max Planck Institute of Colloids and Interfaces.

† Part of the special issue "Arnim Henglein Festschrift".

‡ University of Science and Technology of China. E-mail: shyu@ustc.edu.cn.

§ Max Planck Institute of Colloids and Interfaces. E-mail: coelfen@mpikg-golm.mpg.de.

10.1021/jp034009+ CCC: $25.00
Published on Web 07/12/2003

SCHEME 1: Structure of the Functional Block Copolymer Units[a]

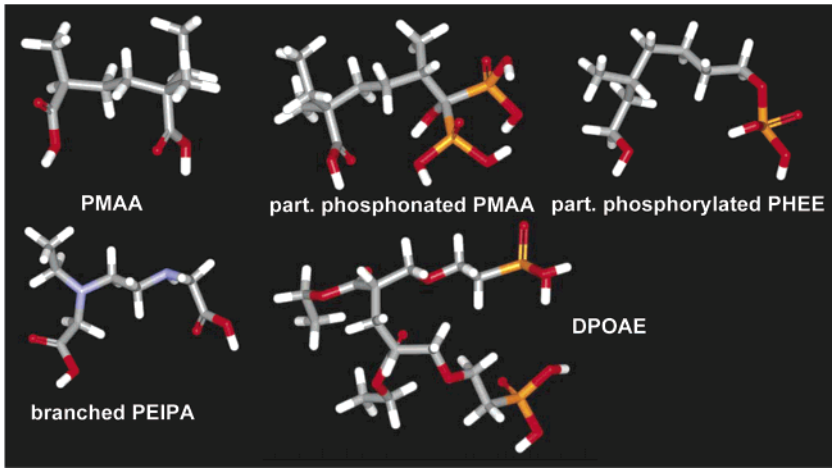

[a] For clarity reasons, the polymers were only drawn as dimeric units. Red, O; yellow, P; gray, C; white, H.

phologies such as hollow spheres composed of calcite rhomboeders were reported, when the DHBCs were combined with surfactants.[48]

In the present study, we examine the structure formation process of various metal carbonate minerals such as $CaCO_3$, $BaCO_3$, $CdCO_3$, $MnCO_3$, and $PbCO_3$ using double hydrophilic block copolymers (DHBCs) with different functional groups as crystal modifiers, revealing details of the mineralization mechanism by cation variation.

2. Experimental Section

All chemicals were obtained from Aldrich and used without further purification. Analytical-grade ammonium carbonate and $CaCl_2$, $BaCl_2$, $CdCl_2$, $MnCl_2$, and $Pb(NO_3)_2$ were used as received. A commercial block copolymer poly(ethylene glycol)-*block*-poly(methacrylic acid) (PEG-*b*-PMAA, PEG = 3000 g mol^{-1}, PMAA = 700 g mol^{-1}) was obtained from Th. Goldschmidt AG, Essen, Germany. PEG-*b*-PMAA polymer was monophosphonated (21%) to give a copolymer with phosphonate groups, PEG-*b*-PMAA-PO_3H_2.[43] A block copolymer containing a poly(ethylenediaminetetraacetic acid) (EDTA)-like carboxy-functionalized block, poly(ethylene glycol)-*block*-poly(ethylene imine)-poly(acetic acid) (PEG-*b*-PEIPA, PEG = 5000 g mol^{-1}, PEIPA = 1800 g mol^{-1}) was synthesized as described elsewhere.[49] The partially phosphorylated poly(hydroxyethylethylene) block copolymer with PEG (PEG-*b*-PHEE-PO_4H_2 (30%)) was synthesized as described in ref 46. A new polymer, PEG-*b*-[(2-[4-dihydroxyphosphoryl]-2-oxabutyl) acrylate ethyl ester] (DPOAE, PEG = 2000 g mol^{-1}), was also applied for crystallization.[50] All copolymers were purified by exhaustive dialysis before use in the crystallization of calcium carbonate.

All glassware (glass bottle and small pieces of glass substrates) was cleaned and sonicated in ethanol for 5 min, then rinsed with distilled water (18 $\Omega M\ cm^{-1}$) and further soaked with a H_2O-HNO_3 (65%)$-H_2O_2$ (1:1:1, v/v/v) solution, then rinsed with doubly distilled H_2O, and finally dried with acetone.

The precipitation of $CaCO_3$ was carried out in glass bottles with volumes of 5−15 mL, which were put into a closed desiccator at room temperature (22 ± 3 °C). A stock aqueous solution of $CaCl_2$ (0.01 M) was freshly prepared in boiled doubly distilled water and bubbled with N_2 overnight before use. Polymer, 30 mg, was added into 30 mL of 0.01 M $CaCl_2$ under vigorous stirring to ensure complete polymer dissolution to generate a 0.01 M $CaCl_2$ solution containing 1 g L^{-1} polymer for further crystallization experiments.

After that, equal volume (10 mL) solutions were added into the glass bottles. The bottles were then covered with Parafilm, which was punched with three needle holes and placed in a larger desiccator. Two small glass bottles (10 mL) of crushed ammonium carbonate were also covered with Parafilm, punched with three needle holes, and placed at the bottom of the desiccator. After different periods of time, the Parafilm was removed, and the precipitate was rinsed with distilled water and ethanol and allowed to dry at room temperature. The time-dependent crystallization experiments were done by taking out the small pieces of glass substrates from the bottles in order to stop the reaction for examination. The initial pH of the solution was about 5. The mineralization of the other carbonates was performed in the corresponding way.

The precipitates were collected and washed with distilled water and dried in air for further characterization. The small pieces of coverslips were examined by optical microscopy and then gold-coated for scanning electron microscopy (SEM) on a DSM 940 A (Carl Zeiss, Jena) microscope. Powder X-ray diffraction (XRD) patterns were recorded on a PDS 120 diffractometer (Nonius GmbH, Solingen) with Cu Kα radiation. The surface cleavage of the crystal faces, the cell structure, and the modeling of polymer were performed with *Cerius*^{2} software (Accelrys).

3. Results and Discussion

The functional units of the block copolymers are shown in Scheme 1 in order to visualize their structure.

Morphosynthesis of $CaCO_3$ via an Aggregation-Based Mechanism. When $CaCO_3$ is crystallized in the presence of PEG-*b*-PMAA with the gas diffusion method, big spherules of about 90 μm are formed after days from spherical rather monodisperse 310-nm precursor particles.[47] Due to the small sample amounts, XRD and FTIR could not be used to identify the crystal modification so that it was deduced from the spherical shape that these precursor particles are composed of nanocrystalline vaterite.[5,43] After a prolonged time, the small spheres were directed to self-assemble into ca. 3-μm spherical structures and a phase transition of vaterite to calcite sets in. After 5 h, hollow spheres were obtained which consist of rhombohedral calcite crystals with well-expressed {10.4} faces with a unit size about 300−400 nm as shown in Figure 1. Figure 1a obviously shows that all those structures are hollow at this stage. The inner part of the hollow structures consists of smaller

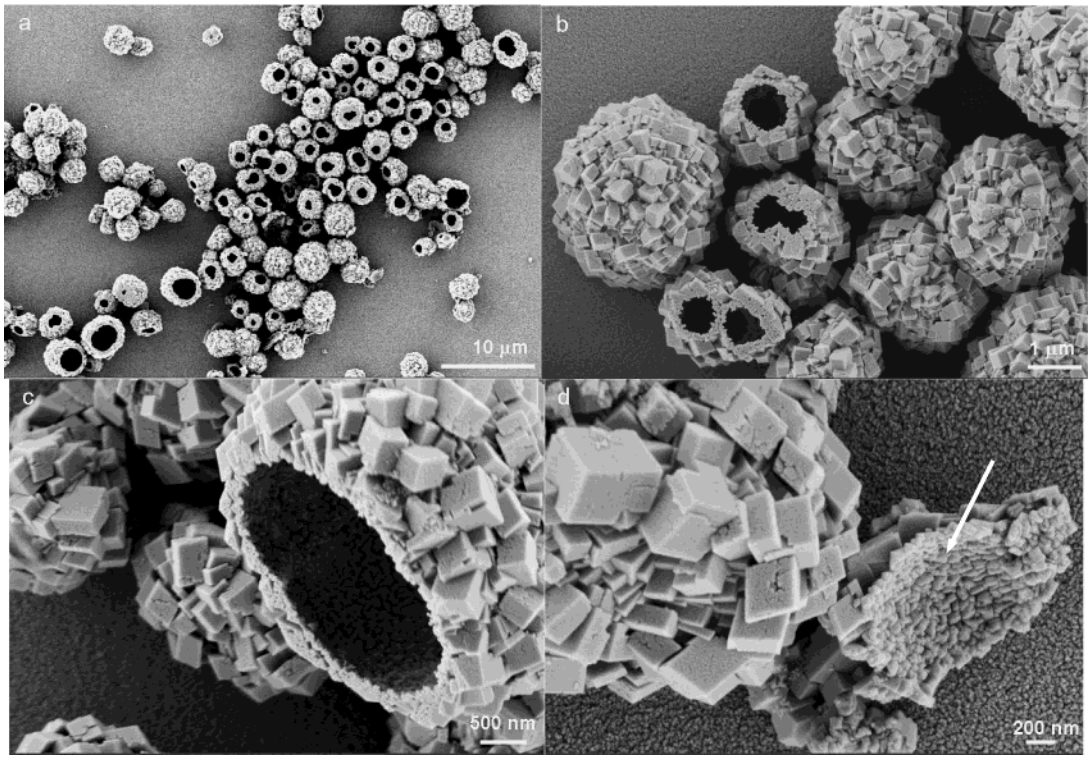

Figure 1. SEM images of $CaCO_3$ particles grown on a glass slip in the early stage, PEG-*b*-PMAA, $[CaCl_2] = 10$ mM, 1 g L^{-1}, 5 h: (a) A full view of $CaCO_3$ particles with either spherical or hollow structures; (b) the surface structure consisted of the calcite rhombohedral subunits with grain size about 320 nm; (c) a typical hollow structure; (d) and the inner structure of the crystals as indicated by the arrow.

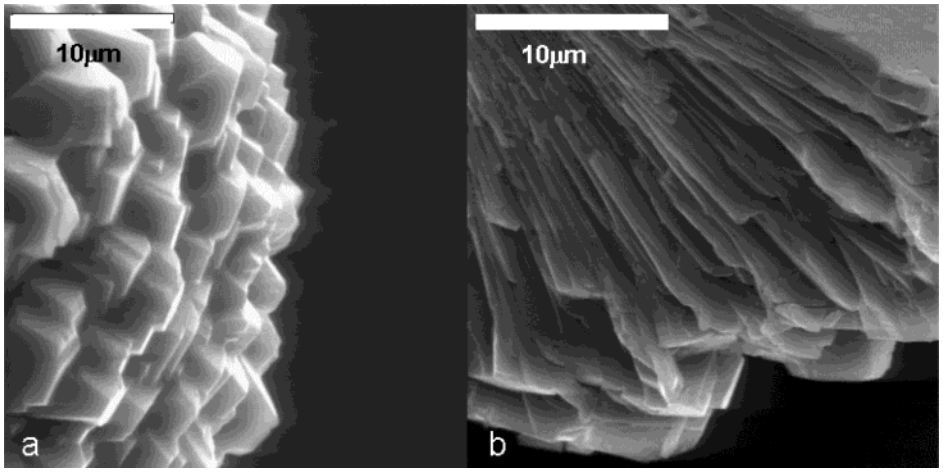

Figure 2. SEM image of (a) the surface structure of a typical $CaCO_3$ spherule grown for 2 weeks, PEG-*b*-PMAA, 1 g L^{-1}, $[CaCl_2] = 10$ mM, (b) and the inner structure of the spherule.

nanoparticles. The size of the inner cavity is remarkably similar to that of the 310-nm spherical precursor particles. Further prolonging the reaction time leads to the formation of big spherules as large as 90 μm and complex surface structures composed of rhombohedral subunits as shown in Figure 2a. Its inner structures display a layered radial growth structure (Figure 2b).

The following growth mechanism can be suggested (Figure 3). At first, vaterite nanospheres form, which subsequently aggregate to ca. 3-μm spherical particles. Later, transformation to calcite beginning on the surface leads to the calcite rhomboeder on the particle surface. These rhomboeders then grow at the expense of the dissolving vaterite particles by Ostwald ripening so that the center of the sphere acts as a sacrifice material depot for the outer calcite particles, resulting in a hollow sphere. Further overgrowth by the much slower process of Ostwald ripening then can lead to the observed radial outgrowth to big spherules with sizes up to 90 μm on the expense of the smaller particles.

It is remarkable that hollow calcite spheres with less expressed surface rhomboeders have been reported[48] only when the same block copolymer was used together with SDS as a second additive. The above-suggested aggregation-based mechanism is rather different from the growth scenarios found for the same system but for faster crystallization conditions which started at a more alkaline pH,[45,51] so that the crystallization kinetics as well as the starting conditions are shown to have a serious influence on the crystal habitus even in the presence of the structure-directing block copolymer. This is not unexpected as the pH is an important variable for $CaCO_3$ polymorph selection

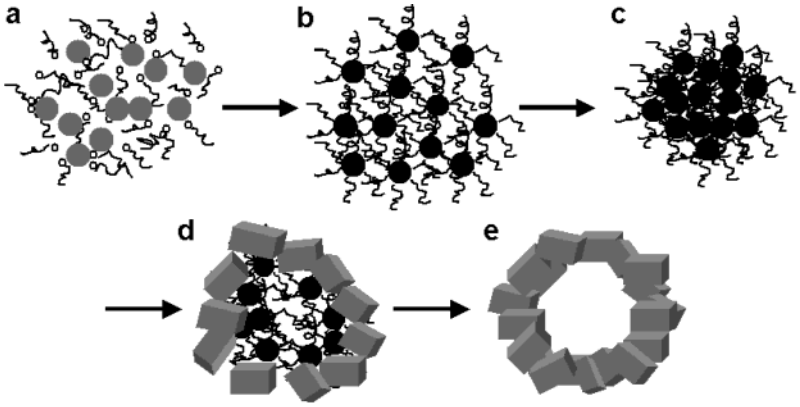

Figure 3. Proposed formation mechanism of the calcite hollow spheres. (a) The polymer-stabilized amorphous nanoparticles; (b) formation of spherical vaterite precursors; (c) aggregation of the vaterite nanoparticles; (d) vaterite−calcite transformation starting on the outer sphere of the particles; (e) formation of calcite hollow spheres under consumption of the vaterite precursors.

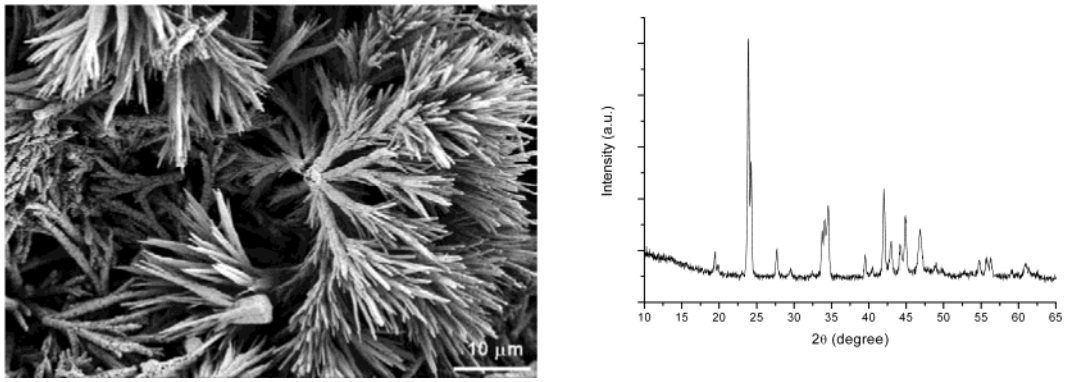

Figure 4. (Left) A typical SEM image shows the dendritic $BaCO_3$ microcrystals obtained on a glass slip by the gas diffusion reaction after 2 weeks. No polymer was added. [$BaCl_2$] = 10 mM. (Right) XRD pattern of the crystals proving the Witherite structure.

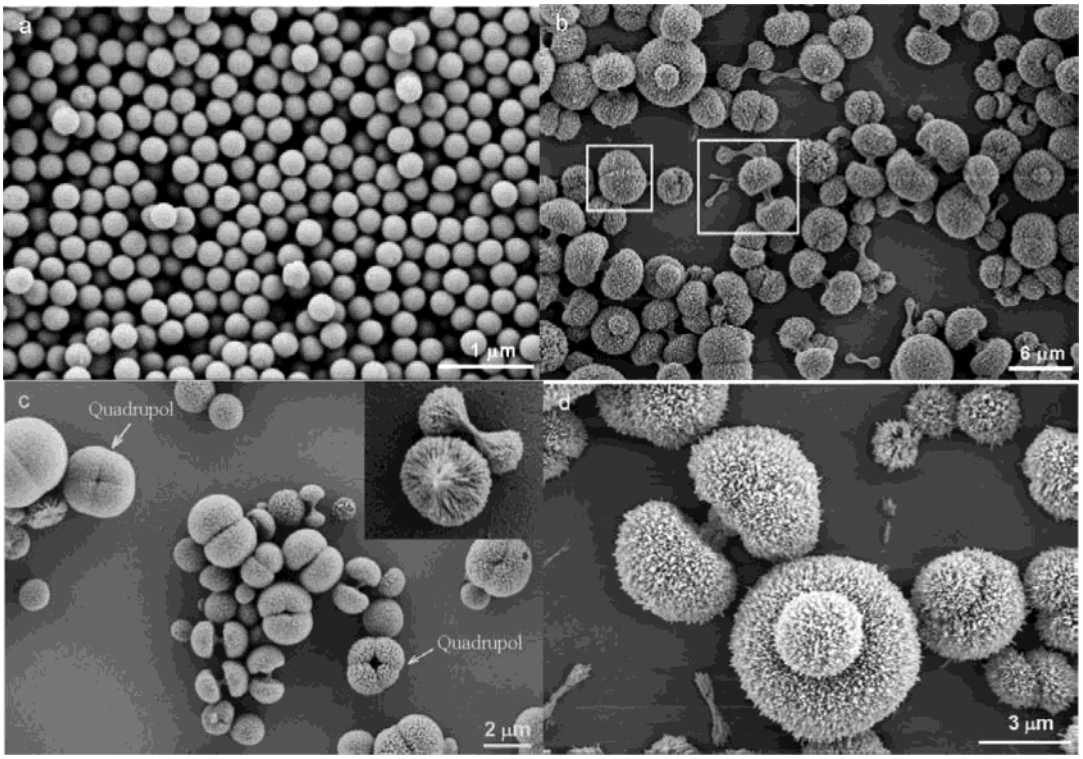

Figure 5. Time-dependent morphology evolution of the $BaCO_3$ crystals obtained in the presence of PEG-*b*-PMAA, [$BaCl_2$] = 10 mM, 1 g L^{-1}, on a glass slip. (a) Primary monodisperse nanospheres with size of 350 nm, 3 h; (b)−(d) 1 day. (b) The coexistence of the different stages of rods, dumbbells, and nearly fully grown spheres; (c) the presence of quadrupolar structures as a defect event. The insert shows a typical fragmented half of a dumbbell and a growing dumbbell; (d) enlarged picture shows detailed structure of the dumbbells with a thin connecting bar.

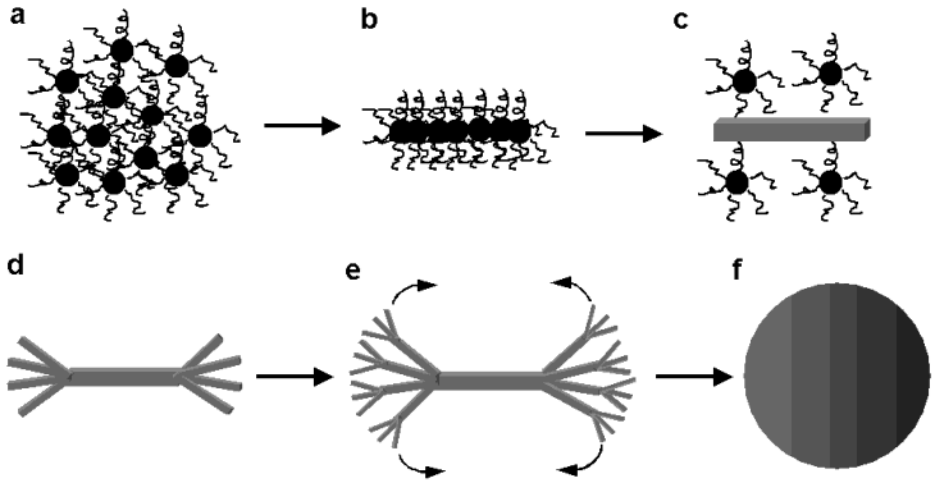

Figure 6. Suggested mechanism for the dendritic growth of a rod (c) formed from spherical precursor structures (a,b) via dumbbell intermediates (d,e) to a final spherical structure (f) based on a mechanism suggested by Busch and Kniep.[53,54]

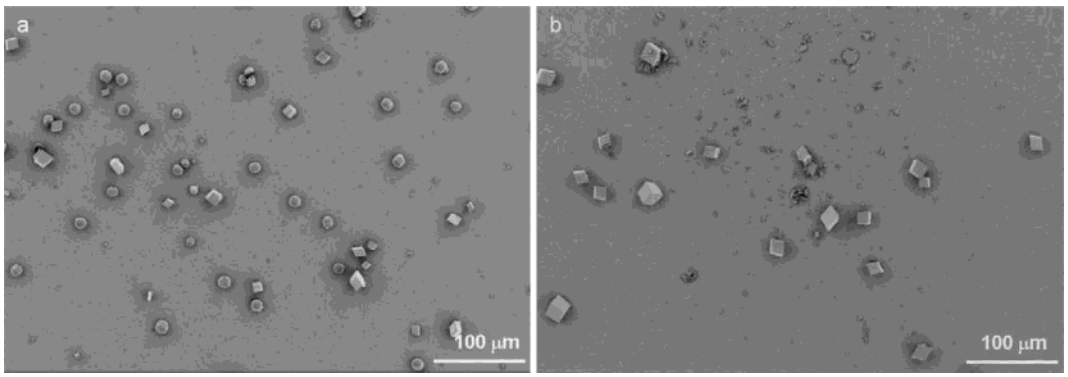

Figure 7. SEM pictures characterizing the salt effects on the crystallization of $CaCO_3$. PEG-*b*-PMAA, $[CaCl_2] = 10$ mM, 1 g L^{-1}, 1 day, on a glass slip. (a) At 0.5 M NaCl, spheres and rhomboeder particles coexist. (b) At 2 M NaCl the inhibition effect of the polymer is totally lost.

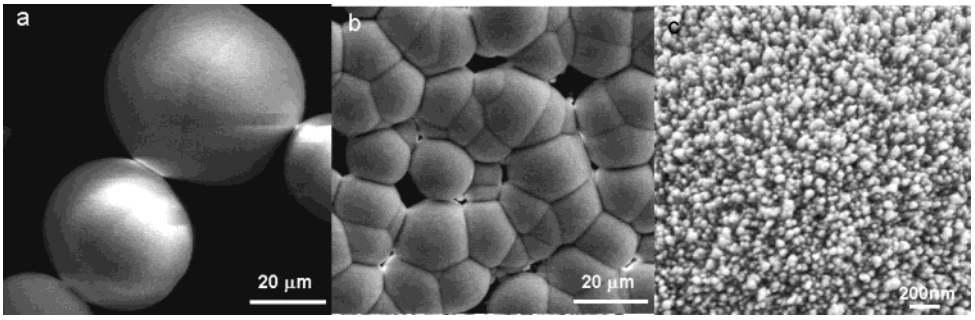

Figure 8. SEM images of big $BaCO_3$ spherules with growth notches formed after 2 weeks in the presence of PEG-*b*-PMAA-PO_3H_2 (21% phosphonation degree), 1 g L^{-1}, pH = 6, $[BaCl_2] = 10$ mM, 2 weeks, PP bottles. (a) Typical spherule; (b) the overgrown spherical aggregates; (c) the surface structure of the crystals.

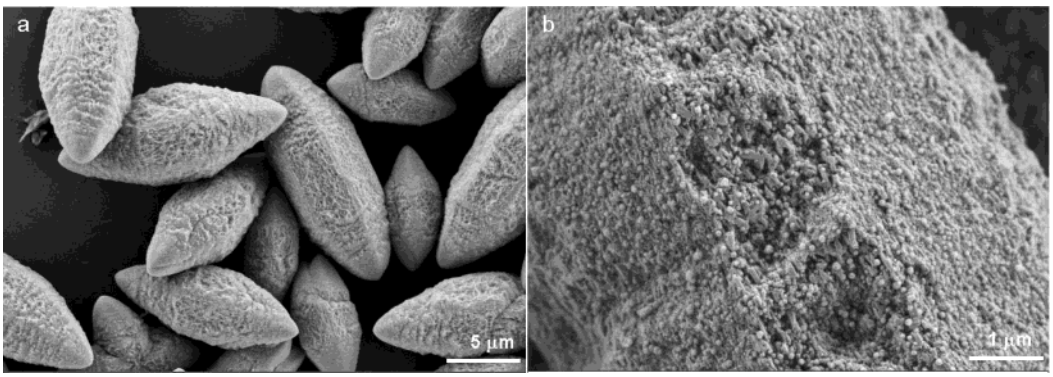

Figure 9. SEM images of the $BaCO_3$ crystals obtained in the presence of PEG-*b*-PHEE-PO_4H_2, pH = 5.5, 1 g L^{-1}, $[BaCl_2] = 10$ mM, 2 days, on a glass slip.

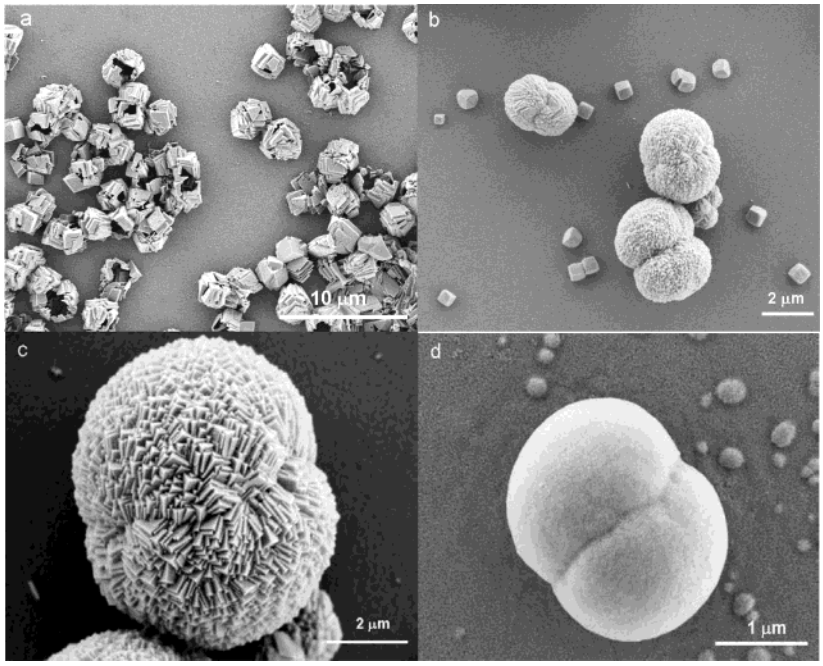

Figure 10. (a) Typical SEM image shows the poorly defined $CdCO_3$ microcrystals obtained on a glass slip by the gas diffusion reaction after 2 weeks without adding DHBCs, $[CdCl_2] = 10$ mM, pH = 5; (b) SEM image of $CdCO_3$ crystals formed in the presence of PEG-*b*-PMAA-PO_3H_2 (1% phosphonation degree), 1 g L^{-1}, $[CdCl_2] = 10$ mM, pH = 5, on a glass slip; (c) an enlarged SEM image shows a typical near sphere growth from dumbbell with densely packed rhomboedric subunits as shown in (b); (d) SEM image of $CdCO_3$ crystals formed in the presence of PEG-*b*-PMAA, 1 g L^{-1}, $[CdCl_2] = 10$ mM, pH = 5, on a glass slip.

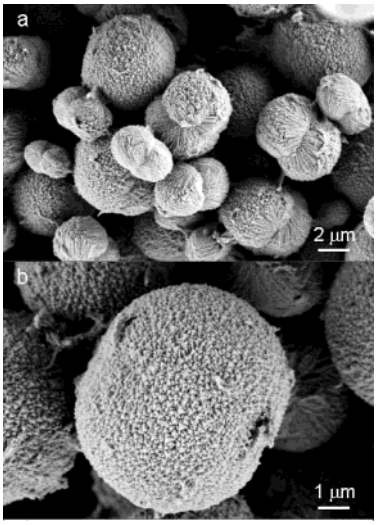

Figure 11. (a) SEM image of $MnCO_3$ crystals formed in the presence of PEG-*b*-[(2-[4-dihydroxyphosphoryl]-2-oxabutyl)acrylate ethyl ester], 1 g L^{-1}, pH = 4, $[MnCl_2] = 10$ mM, 2 weeks, on a glass slip.

where the higher pH values favor calcite over vaterite.[52] The more acidic starting conditions in this study may favor initial vaterite growth, whereas the steadily increasing pH will lead to calcite at a later experimental stage.

Morphosynthesis of $BaCO_3$ via a Sphere−Rod−Dumbbell−Sphere Growth Process. Morphosynthesis of the homologue $BaCO_3$ (orthorhombic structure; space group *Pnma*) can also be successfully controlled by DHBCs. Figure 4 shows the dendritic $BaCO_3$ (Witherite) crystals formed in the absence of block copolymer. The XRD pattern in Figure 4 underlines that the system adopted the orthorhombic structure with cell constants $a = 5.31$, $b = 8.9$, $c = 6.43$.

Similar to the case of $CaCO_3$, highly monodisperse $BaCO_3$ nanospheres with a size of 350 nm were obtained 3 h after the start of the gas diffusion reaction (Figure 5a). With increasing

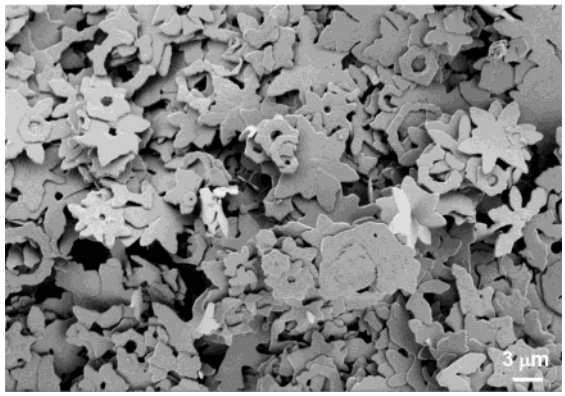

Figure 12. $PbCO_3$ crystals obtained by the gas diffusion technique after reaction for 2 weeks (without additives).

reaction time, these structures disappear, and a coexisting family of rods, dumbbells, and fully grown spheres appears as shown in Figure 5, suggesting a morphology transition of the "sphere-to-rod-to-dumbbell-to-sphere" upon growth as illustrated in Figure 6. This mechanism was already described for the growth of fluoroapatite in gelatin gels,[53,54] except that in the present case of a free solution instead of a gelatin gel, the different stages of particle growth are coexisting. Interestingly, some quadrupole shaped crystals were also found Figure 5c. Although the crystal growth is already dendritic without additives, the sphere−rod−dumbbell−sphere transition is only observed in the presence of the block copolymer. While the sphere−rod−dumbbell−sphere transition seems to be a general growth phenomenon and was observed for several systems, the exact growth mechanism is unknown, although some explanation was given in the literature based on the role of intrinsic electric fields which direct the growth of dipole crystals.[51,54]

To check for the role of Coulombic interactions in both mineralization scenarios, the influence of increasing the ionic strength of the solution via addition of an inert salt was tested. For the $CaCO_3$ case, mineralization in 0.5 M NaCl solution

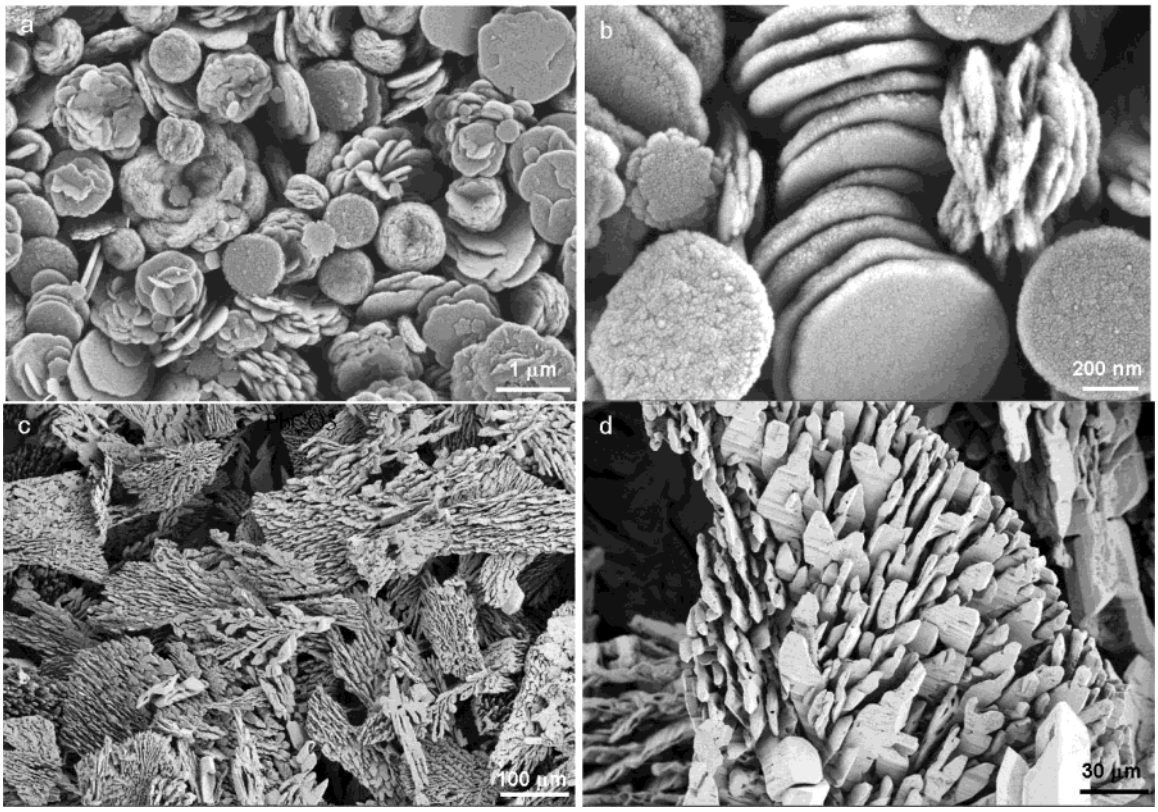

Figure 13. Time-dependent morphology evolution of $PbCO_3$ crystals obtained in the presence of PEG-*b*-PMAA, $[Pb(NO_3)_2] = 10$ mM, 1 g L^{-1}, on a glass slip. (a)−(b) Nanoplates formed, 3 h; (c)−(d) superstructures formed after 2 weeks.

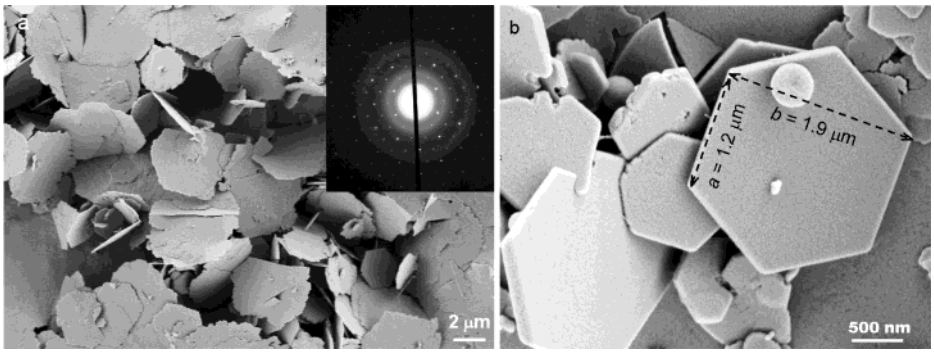

Figure 14. (a) SEM image of $PbCO_3$ nanoplates formed after 2 weeks, PEG-*b*-[(2-[4-dihydroxyphosphoryl]-2-oxabutyl)acrylate ethyl ester], 1 g L^{-1}, pH = 5.6, $[Pb(NO_3)_2] = 10$ mM, 2 weeks, on a glass slip. Insert shows the electron diffraction pattern of the nanoplates taken perpendicular to the ⟨001⟩ plane; (b) a SEM image shows the ripened elongated quasi-hexagonal nanoplates with a typical thickness of 90 nm. Note that this phosphonated polymer keeps the hexagonal plates long-term stable.

shows the coexistence of spherules with rhomboeders in solution (Figure 7a). Further increase of the concentration of NaCl up to 2 M results in the complete disappearance of the spherules as shown Figure 7b, implying that the morphology-directing effect of the polymer is lost.

This influence can be partly attributed to the salting out of the PMAA polymer block at higher ionic strengths, which leads to polymer aggregation,[55] thus decreasing the block copolymer activity for interaction with the crystal surface. As the influence of the ionic strength itself was found to be negligible to determine the polymorph of $CaCO_3$,[52] it is most unlikely to be the reason for the observed morphology changes by itself.

Astonishingly, if the same experiment is repeated with $BaCO_3$, no influence of the inert salt on the morphology is found. This means on one hand that the binding between polymer and Ba mineral surfaces is much stronger and that even the partly aggregated DHBCs can exert a morphology-directing action. On the other hand, we can virtually exclude that the found dumbbell fractal structure is due to the action of a long-range electric field throughout solution, as the Debye length characterizing the extension of the electric double layer is virtually zero in 2 M NaCl. This experiment refutes the previous interpretation and leaves the explanation for the formed fractal structure wide open.

When the PEG-*b*-PMAA is partially phosphonated, the morphology of the formed $BaCO_3$ is different from that in Figure 5. Although big spherical superstructures or their aggregates are obtained with PEG-*b*-PMAA-PO_3H_2 (21%) as additive (Figure 8a), too, the surfaces of the structures consisted of fine nanoparticles with a primary grain size of 40 nm, as shown in Figure 8c. Compared to the polymer with carboxyl functionalities, the phosphonated polymer seems to stabilize smaller crystalline units due to its stronger interaction with the crystals, so that the surface is more smooth, although the overall growth mechanism may be similar. When PEG-*b*-PEIPA was used as additive, similar superstructures but with rough surface structure

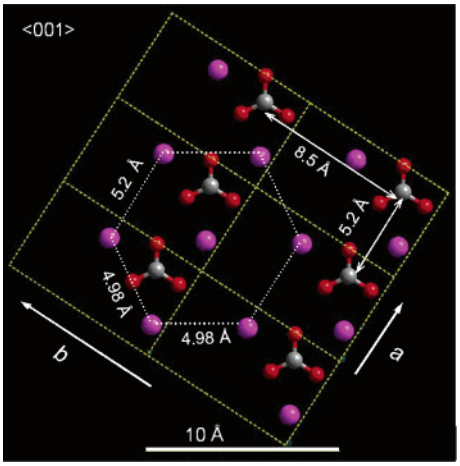

Figure 15. View along the ⟨001⟩ axis of the cleaved surface of the {00.1} face, which was done by Cerius[2] software, showing the uniaxially elongated hexagonal arrangement of Pb ions within the {00.1} surface. Magenta, Pb; red ball, O; gray, C.

can be obtained, underlining that the surface structures can be well controlled by the chemical functionalities and the coupled binding strengths of DHBCs.

A new morphology which does not fit in the line was generated with the partially phosphorylated poly(hydroxyethylethylene) block copolymer (PEG-*b*-PHEE-PO_4H_2 (30%)). Here, exclusively oval crystals of length 8−30 μm are generated as shown in Figure 9a. The objects look like dense, well-crystallized species (note that the base system just forms dendritic structures), but this must be confirmed with a microfocus X-ray experiment. The enlarged SEM image in Figure 9b shows that the crystals are at least overgrown with densely packed, fine nanocrystals with a size of about 60 nm.

The "nonsystematic" behavior of this polymer is speculatively explained by a break-up of the standard growth scenario by this polymer, i.e., as indicated by the strongly increased crystal size, not only growth, but especially nucleation is strongly suppressed by this polymer.

Morphosynthesis of $CdCO_3$ and $MnCO_3$. To verify the above "sphere−rod−dumbbell−sphere" transformation process, a similar mineralization reaction was applied to otavite ($CdCO_3$) and rhodochrosite ($MnCO_3$), which are structural homologues of calcite. Figure 10a shows that poorly defined otavite particles with sizes around 3−5 μm which display {10.4} faces are obtained when no polymer is added. Interestingly, already those "default structures" are hollow, indicating the existence of a rapidly precipitating but metastable intermediate which is sacrificed throughout further morphology development.

In the presence of weakly phosphonated PEG-*b*-PMAA (1% degree of phosphonation), the coexistence of smaller, 500 nm, rhombohedral nanocrystals (presumably uncontrolled growth) and the already well-known dumbbells with an overall size of 2−3 μm were found in the early stage of the gas diffusion reaction (Figure 10b). It is worth mentioning that the small rhombohedral nanocrystals are disappearing with time, indicating that the polymer protected dumbbells have a lower surface free energy than the free rhombohedral species. The detailed surface structure of a typical nearly fully grown dumbbell is shown in Figure 10c, illustrating the intercalated structure of the constituting rhombohedral subunits. A similar growth scenario was obtained with the pure PEG-*b*-PMAA. In the early stages of the reaction, both smaller precursor structures and dumbbells with a very fine surface texture are formed (Figure 10d). With increasing time, big spherical aggregates with an overall size of 2−3 μm and a textured surface are formed again.

A very similar growth scenario and coupled zoo of well-defined species was also formed for $MnCO_3$. Figure 11a shows that both 3−5 μm big dumbbells and spheres can be readily produced in the presence of PEG-*b*-[(2-[4-dihydroxyphosphoryl]-2-oxabutyl)acrylate ethyl ester]. Such $MnCO_3$ structures with complex subunits on the surface were previously not realized, as either the reaction of $MnSO_4$ with NH_4HCO_3 in solution[56] or the reaction of $MnSO_4$ with urea by aging at elevated temperatures[57] produced rhombohedral particles. These results also imply that the rod−dumbbell−sphere morphogenesis can be observed for many metal carbonate systems, indicating a universal underlying mechanism.

Morphosynthesis of $PbCO_3$ by Stabilization of a Single Plane. Last, we examine the growth processes of $PbCO_3$ (Cerussite, orthorhombic structure with space group *Pmcn*). Gas diffusion reaction in the absence of block copolymers leads to poorly defined starlike $PbCO_3$ cerussite platelets (cell constants $a = 5.178$, $b = 8.515$, $c = 6.146$ Å), as shown in Figure 12.In the presence of PEG-*b*-PMAA, disklike nanoplates with diameter of 600 nm and a thickness of 50 nm are formed as the primary, short-term structure. Some of the plates branch or stack together to form complex structures as shown in Figure 13a,b. The plates are, however, just structural intermediates, as with increasing time, bigger aggregates with a scuted surface structure are formed (Figure 13c,d).

It is also interesting to speculate about the physicochemical reason for the very well-defined thickness of 50 nm of the otherwise strictly two-dimensional crystalline objects. One explanation is that the two ⟨001⟩ faces repell each other, e.g., either by Coulombic forces through the crystal or by mechanical stress fields due to surface reconstitution. The found 50 nm would then be the minimal distance to place two such ⟨001⟩ faces in a crystal or, in other words, the "thickness" of the surface-controlled phase layer would be 25 nm in $PbCO_3$. This is an unexpectedly high value.

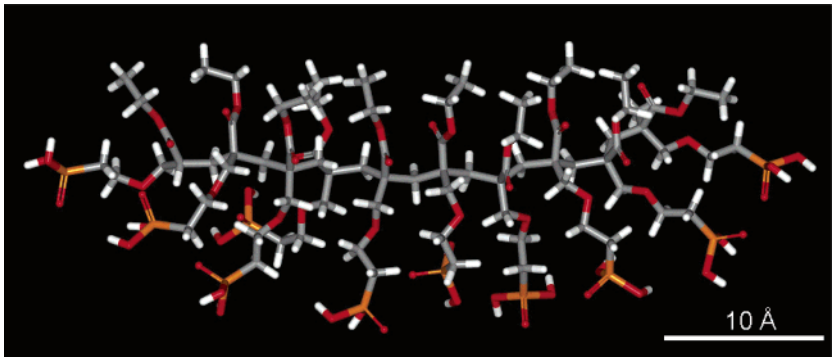

Figure 16. Computer modeling results of the vacuum energy minimum conformation of the functional block of PEG-*b*-[(2-[4-dihydroxyphosphoryl]-2-oxabutyl)acrylate ethyl ester] in a vacuum. The modeling was done with the Cerius[2] software. Red, O; yellow, P; gray, C; white, H.

With our tool of systematic increase of binding strength with increased amount of phosphonation, it is possible to stabilize the interesting $PbCO_3$ platelet-like intermediates permanently. When the strong binder PEG-*b*-[(2-[4-dihydroxy phosphoryl]-2-oxabutyl)acrylate ethyl ester] was used, flat sheetlike particles with a smooth surface and a thickness of about 90 nm were obtained as shown in Figure 14a. The insert electron diffraction pattern taken along ⟨001⟩ shows its single crystalline nature, corresponding to uniaxially elongated quasi-hexagonal nanoplates.

The selected but typical uniaxially elongated quasi-hexagonal nanoplates shown in Figure 14b are in fact the outside embodiment of the cerussite cell structure with an *a*/*b* ratio of about 0.6, which fits the modeling result by Cerius[2] impressively well. Figure 15 shows the conformation of the Pb^{2+} ions and CO_3^{2-} ions viewed along the ⟨001⟩ axis. It becomes obvious that the crystals grew preferentially along the *a* and *b* axes. XRD patterns also support these results, as stronger (*hk*0) diffraction peaks and weaker (002) diffraction peaks as compared to the default mineral are found. Again, it is worth mentioning that the thickness of the structures is practically constant at about 90 nm; that is, the polymer adsorption does not decrease the platelet thickness (as it would be expected by a simple blocking mechanism) but obviously even increases the surface−surface repulsion. A further clarification of this effect must be the subject of forthcoming work.

The only possibility to explain the perfection of the crystals in the presence of this DHBC and all other effects is a site-selective absorption of the functional groups on the ⟨001⟩ faces. An energy-minimized computer structure of the functional head block of PEG-*b*-[(2-[4-dihydroxy phosphoryl]-2-oxabutyl)acrylate ethyl ester] in a vacuum is illustrated in Figure 16, showing the phosphonate binding sites in a variety of distances between 5 and 8 Å. This matches the distances between nearby lead ions of 5.2, 5.0, and 8.5 Å, as shown in Figure 15; that is, the polymer can at least adsorb onto the ⟨001⟩ face without too much loss of conformational entropy. The reason this special block copolymer is so special in its inhibition of inorganic crystal growth is, however, not clarified by such a plausibility argumentation, and more detailed results will be reported in future.

4. Conclusions

In summary, different morphosynthesis strategies for metal carbonates with well-defined surface structures by using DHBCs as crystal modifiers were presented. Apparently, the same set of molecules can adopt different functions ranging from the temporary stabilization of precursor phases over directed crystal growth to face selective adsorption. This is a toolbox for the generation of complex morphologies which operates up to now just in a systematic, but phenomenological, way, as it is still not possible to predict the morphologies for unknown mineral systems from the used additive. Nevertheless, some archetypical, common growth scenarios exist as the rod−dumbbell−sphere growth mechanism, which was previously described for fluoroapatite[53,54] but is now described also for several metal carbonate systems such as $CaCO_3$, $BaCO_3$, $CdCO_3$, and $MnCO_3$.

It was also found that the inhibition ability of the DHBCs was lost for $CaCO_3$ when the ionic strength was increased by adding NaCl to the system but prevailed for the Ba species. From these experiments, we can exclude the influence of long-ranged Coulombic forces as a structure-directing element in those mineralization reactions.

The successful realization of the biomimetic morphogenesis of different minerals by using double-hydrophilic block copolymers as crystal growth modifiers extends the possibilities of previous attempts of inorganic morphogenesis. The results suggest that DHBC copolymers with more complex patterns of chemical groups may provide even more effective tools for the controlled synthesis of inorganic crystals.

Acknowledgment. We thank the Max Planck Society and DFG (SFB448) for funding. S.-H. Yu thanks the Alexander von Humboldt Foundation for supporting his research stay in Germany and the special funding support from the Century Program of the Chinese Academy of Sciences. H. C. thanks the Dr. Hermann Schnell Foundation for financial support. We thank Dr. Jürgen Hartmann and Ms. Rona Pitschke for their skillful SEM measurements. Dr. Klaus Tauer is thanked for leaving the PEG-*b*-DPOAE block copolymer at our deposition and Th Goldshimidt AG, Essen, Germany, is thanked for the generous gift of PEG-*b*-PMAA.

References and Notes

(1) See review and references therein: (a) Mann, S. *Angew. Chem., Int. Ed. Engl.* **2000**, *39*, 3392. (b) Estroff, L. A.; Hamilton, A. D. *Chem. Mater.* **2001**, *13*, 3227.

(2) Dalas, E.; Klepetsanis, P.; Koutsoukos, P. G. *Langmuir* **1999**, *15*, 8322.

(3) Falini, G.; Albeck, S.; Weiner, S.; Addadi, L. *Science* **1996**, *271*, 67.

(4) DeOliveira, D. B.; Laursen, R. A. J. *Am. Chem. Soc.* **1997**, *119*, 10627.

(5) Cölfen, H. *Curr. Opin. Colloid Interface Sci.* **2003**, *8*, 23.

(6) Mann, S.; Heywood, B. R.; Rajam, S.; Birchall, J. D. *Nature* **1988**, *334*, 692.

(7) Didymus, J. M.; Mann, S.; Benton, W. J.; Collins, I. R. *Langmuir* **1995**, *11*, 3130.

(8) Ahn, D. J.; Berman, A.; Charych, D. *J. Phys. Chem.* **1996**, *100*, 12455.

(9) Litvin, A. L.; Valiyaveettil, S.; Kaplan, D. L.; Mann, S. *Adv. Mater.* **1997**, *9*, 124.

(10) Lahiri, J.; Xu, G. F.; Dabbs, D. M.; Yao, N.; Aksay, I. A.; Groves, J. T, *J. Am. Chem. Soc.* **1997**, *119*, 5449.

(11) Archibald, D. D.; Qadri, S. B.; Gaber, B. P. *Langmuir* **1996**, *12*, 538.

(12) Kuther, J.; Nelles, G.; Seshadri, R.; Schaub, M.; Butt, H. J.; Tremel, W. *Chem. Eur. J.* **1998**, *4*, 1834. Küther, J.; Tremel, W. *J. Chem. Soc., Chem. Commun.* **1997**, 2029. Küther, J.; Seshadri, R.; Knoll, W.; Tremel, W. *J. Mater. Chem.* **1998**, *8*, 641.

(13) Aizenberg, J.; Black, A. J.; Whitesides, G. M. *Nature* **1999**, *398*, 495.

(14) Aizenberg, J.; Black, A. J.; Whitesides, G. M. *J. Am. Chem. Soc.* **1999**, *121*, 4500.

(15) Chen, B. D.; Cilliers, J. J.; Davey, R. J.; Garside, J.; Woodburn, E. T. *J. Am. Chem. Soc.* **1998**, *120*, 1625.

(16) Falini, G.; Fermani, S.; Gazzano, M.; Ripamonti, A. *Chem. Eur. J.* **1997**, *3*, 1807.

(17) Falini, G.; Fermani, S.; Gazzano, M.; Ripamonti, A. *Chem. Eur. J.* **1998**, *4*, 1048.

(18) D'Souza, S. M.; Alexander, C.; Carr, S. W.; Waller, A. M.; Whitcombe, M. J.; Vulfson, E. N. *Nature* **1999**, *398*, 312.

(19) Loste, E.; Meldrum, F. C. *Chem. Commun.* **2001**, 901.

(20) Park R. J.; Meldrum, F. C. *Adv. Mater.* **2002**, *14*, 1167−1169.

(21) Didymus, M.; Oliver, P.; Mann, S.; DeVries, A. L.; Hauschka, P. V.; Westbroek, P. *J. Chem. Soc., Faraday Trans.* **1993**, *89*, 2891.

(22) T. Kato, T. Suzuki, T. Amamiya, T. Irie, M. Komiyama, H. Yui, *Supramol. Sci.* **1998**, *5*, 411.

(23) Naka, K.; Tanaka, Y.; Chujo, Y. I. *Chem. Commun.* **1999**, 1931.

(24) Gower, L. A.; Tirrell, D. A. *J. Cryst. Growth* **1998**, *191*, 153.

(25) Gower L. B.; Odom, D. J. *J. Crystal Growth* **2000**, *210*, 719.

(26) Donners, J. J. J. M.; Heywood, B. R.; Meijer, E. W.; Nolte, R. J. M.; Roman, C.; Schenning, A. P. H. J.; Sommerdijk, N. A. J. M. *Chem. Commun.* **2000**, 1937.

(27) Donners J. J. J. M.; Heywood, B. R.; Meijer, E. W.; Nolte, R. J. M.; Sommerdijk N. A. J. M. *Chem. Eur. J.* **2002**, *8*, 2561.

(28) Xu, G.; Yao, N.; Aksay, I. A.; Groves, J. T. *J. Am. Chem. Soc.* **1998**, *120*, 11977.

(29) Zhang, S.; Gonsalves, K. E. *Langmuir* **1998**, *14*, 6766.

(30) Levi, Y.; Albeck, S.; Brack, A.; Weiner, S.; Addadi, L. *Chem. Eur. J.* **1998**, *4*, 389.

(31) Belcher, A. M.; Wu, X. H.; Christensen, R. J.; Hansma, P. K.; Stucky, G. D.; Morse, D. E. *Nature* **1996**, *381*, 36.
(32) Aizenberg, J.; Hanson, J.; Koetzle, T. F.; Weiner, S.; Addadi, L. *J. Am. Chem. Soc.* **1997**, *119*, 881.
(33) Aizenberg, J.; Lambert, G.; Weiner, S.; Addadi, L. *J. Am. Chem. Soc.* **2002**, *124*, 32.
(34) Li, C. M.; Botsaris, G. D.; Kaplan, D. L. *Crystal Growth Design* **2002**, *2*, 387.
(35) Lee, I.; Han, S. W.; Choi, H. J.; Kim, K. *Adv. Mater.* **2001**, *13*, 1617.
(36) Küther, J.; Seshadri, R.; Tremel, W. *Angew. Chem., Int. Ed. Engl.* **1998**, *37*, 3044. Küther, J.; Seshadri, R.; Nelles, G.; Assenmacher, W.; Butt, H.-J.; Mader, W.; Tremel, W. *Chem. Mater.* **1992**, *4*, 1834.
(37) For a recent review see: Cölfen, H. *Macromol. Rapid Commun.* **2001**, *22*, 219.
(38) Sedlak, M.; Antonietti, M.; Cölfen, H. *Macromol. Chem. Phys.* **1998**, *199*, 247.
(39) Kaluzynski, K.; Pretula, J.; Lapienis, G.; Basko, M.; Bartczak, Z.; Dworak, A.; Penczek, S. *J. Polym. Sci: Part A: Polym. Chem.* **2001**, *39*, 955.
(40) Ershow, B. G.; Henglein, A. *J. Phys. Chem. B* **1998**, *102*, 10663.
(41) Gutierrez, M.; Henglein, A. *J. Phys. Chem.* **1996**, *100*, 7656.
(42) Henglein, A.; Linnert, T.; Mulvaney, P. *Ber. Bunsen Phys. Chem.* **1996**, *94*, 1449.
(43) Cölfen, H.; Antonietti, M. *Langmuir* **1998**, *14*, 582.
(44) Marentette, J. M.; Norwig, J.; Stockelmann, E.; Meyer, W. H.; Wegner, G. *Adv. Mater.* **1997**, *9*, 647.
(45) Cölfen, H.; Qi, L. M. *Chem. Eur. J.* **2001**, *7*, 106.
(46) Rudloff, J.; Antonietti, M.; Cölfen, H.; Pretula, J.; Kaluzynski, K.; Penczek, S. *Macromol. Chem. Phys.* **2002**, *203*, 627.
(47) Yu, S. H.; Cölfen, H.; Hartmann, J.; Antonietti, M. *Adv. Funct. Mater.* **2002**, *12*, 541.
(48) Qi, L. M.; Li, J.; Ma, J. M. *Adv. Mater.* **2002**, *14*, 300.
(49) Sedlak, M.; Cölfen, H. *Macromol. Chem. Phys.* **2001**, *202*, 587.
(50) Yu, S. H.; Cölfen, H.; Tauer, K.; Antonietti, M., unpublished.
(51) Cölfen, H.; Qi, L. *Prog. Colloid Polym. Sci.* **2001**, *11*, 200.
(52) Tai, C. Y.; Chen, F. B. *AlChE J.* **1998**, *44*, 1790.
(53) Kniep, R.; Busch, S. *Angew. Chem., Int. Ed. Engl.* **1996**, *35*, 2624.
(54) Busch, S.; Dolhaine, H.; DuChesne, A.; Heinz, S.; Hochrein, O.; Laeri, F.; Podebrad, O.; Vietze, U.; Weiland, T.; Kniep, R. *Eur. J. Inorg. Chem.* **1999,** 1643.
(55) Philipp, B.; Dautzenberg, H.; Linkow, K. J.; Kötz, J.; Dawydoff, W. *Prog. Polym. Sci.* **1989**, *14*, 91.
(56) Hamada, S.; Kudo, Y.; Okada, J.; Kano, H. *J. Colloid Interface Sci.* **1987**, *118*, 356.
(57) Haq, I.; Matijevic, E. *Chem. Mater.* **1997**, *9*, 2659.